Molecular electronics using diazonium-derived adlayers on carbon with Cu top contacts: critical analysis of metal oxides and filaments

2008 J. Phys.: Condens. Matter 20 374117

(http://iopscience.iop.org/0953-8984/20/37/374117)

J. Phys.: Condens. Matter **20** (2008) 374117 (11pp) doi:10.1088/0953-8984/20/37/374117

Molecular electronics using diazonium-derived adlayers on carbon with Cu top contacts: critical analysis of metal oxides and filaments

Adam Johan Bergren[1], **Kenneth D Harris**[1], **Fengjun Deng**[2] **and Richard L McCreery**[1,2,3]

[1] National Institute for Nanotechnology, National Research Council Canada, Edmonton, Alberta, Canada
[2] Department of Chemistry, University of Alberta, Edmonton, Alberta, Canada

E-mail: Adam.Bergren@nrc.ca and richard.mccreery@ualberta.ca

Received 29 February 2008, in final form 9 April 2008
Published 26 August 2008
Online at stacks.iop.org/JPhysCM/20/374117

Abstract

Evaporation of Cu metal onto thin (less than 5 nm) molecular layers bonded to conductive carbon substrates results in electronic junctions with an ensemble of molecules sandwiched between two conductors. The resulting devices have previously been characterized through analysis of current density–voltage (j–V) curves for several different molecular layers and as a function of layer thickness. The approach represents an 'ensemble' rather than 'single molecule' technique, in which the electronic response represents that of a large number of molecules (10^6–10^{12}) in parallel as well as the conducting contacts contained in the molecular junction. In this paper, we extend a more detailed investigation of two critical issues: the possibility of conduction by metal filaments, and the potential role of top contact oxidation contributing to the electronic properties of the junctions. The results show that the conductance of the junctions can be modulated by changes in the deposition environment, but that the changes are not related to Cu oxide in the top contact. Based on these results, we propose that the conditions during top contact deposition change the way in which the molecules contact the metal, leading to differences in the effective junction area. Finally, through systematic studies using variation of the temperature, we show that metal filament conduction is distinct from that observed for the molecular junctions and that if the current observed experimentally passed through nanoscopic metal filaments the Joule heating would lead to rapid melting. For a series of junctions with structurally related aromatic molecules (including biphenyl, nitrobiphenyl, fluorene, and nitroazobenzene), the electron transfer mechanism is briefly investigated using area-independent analysis methods. It is shown that field emission and/or transport through bands formed by the molecular layer is likely, based on the weak temperature dependence of junction conductance.

S Supplementary data are available from stacks.iop.org/JPhysCM/20/374117

1. Introduction

Despite a large effort in the field of molecular electronics, there is much debate regarding the importance of contacts in determining the behaviour of a molecular junction [1–5]. Even when novel behaviours such as conductance switching [6] and negative differential resistance [7, 8] are demonstrated, or when the overall electron transfer mechanism is determined (i.e. tunnelling, field emission, etc), there is often uncertainty about what role is played by the contacts. In order to overcome this obstacle, various strategies have been employed, including a wide range of techniques for junction fabrication and the

[3] Author to whom any correspondence should be addressed.

design of appropriate control experiments [9–12]. However, clarification of the contact issue is hindered since there is a multitude of mechanisms by which a molecule can be anchored to a conductive surface, including different covalent linkage schemes along with attachment modes that rely on non-covalent interactions [13]. Moreover, many fabrication techniques rely on the deposition of a conductive 'top contact' to complete the device. The electronic coupling between the molecules and the contacts at both molecule/contact interfaces can therefore be dependent upon the techniques used to construct the device, which, in turn, can affect the overall electronic behaviour of the molecular junction.

Our laboratory has recently reported the characteristics of several types of molecular electronic junctions made by electron-beam evaporation of metallic top contacts onto molecular layers bonded to flat carbon substrates [1, 14–27]. Modification of a conductive carbon surface (prepared by the pyrolysis of photoresist and known as pyrolysed photoresist film, PPF) [28] is accomplished via the reduction of diazonium reagents [29–32], leading to the formation of 1–5 nm thick molecular mono- or multilayers [33, 34] anchored by carbon–carbon bonds. Through this paradigm, different types of carbon–molecule–metal or carbon–molecule–metal oxide–metal junctions have been investigated [1, 14–24, 26–28]. Importantly, high yield and reproducibility can be achieved using this junction design, enabling systematic studies of various aspects of device behaviour with a high degree of certainty that junction behaviour is not an artefact of uncontrolled experimental parameters. Characterization of junctions containing Ti and Cu top contacts [20, 22] reveals that in some cases a covalent bond is formed between the top contact metal and the molecular layer. In such instances, both contacts have covalent linkages to the molecular layer. However, the identity and oxidation state of the top contact can have a large influence on the characteristics of the device such that changes in junction conductivity over time and specialized behaviour like rectification or hysteresis were observed in junctions containing metal oxides. In this paper, we extend these studies by presenting a detailed description of carbon–molecule–metal molecular junctions prepared using Cu as the top contact, with a focus on fabrication details and how molecular structure impacts junction conductance.

The molecular junctions fabricated in our laboratory are 'large area' junctions that contain an ensemble of 10^6–10^{12} molecules in parallel. Several methods exist for fabricating such devices, including deposition of metals onto molecule-modified substrates [21, 35, 36], spin-coating conductive polymers onto self-assembled monolayers (SAMs) on various metals [37, 38], the use of Hg contacts [39], and others [1, 11, 18]. There are also a variety of techniques for studying devices where only single molecules or small clusters of molecules are contained within the junction [2, 40, 41]. It is notable that the conductance per molecule appears to change drastically with the total number of molecules in a junction, as recently reviewed [42]. This 'scaling issue' seems to depend not only on the number of molecules in the device, but also on the way in which the junction is fabricated (including how contacts are made). Ensemble, or 'large area', devices present a different set of problems [11, 36, 37] compared to those encountered in single molecule devices [3–5]. Two critical issues arise when depositing top contacts via evaporation of metals onto large area junctions: the possible oxidation of the metal and the formation of metallic filaments as 'short circuits' that bypass possible conduction through the molecules. In the current report, we consider the conditions during top contact deposition in order to extend our previous work on carbon–molecule–Cu junctions [15, 22] and qualify the behaviour of ensemble junctions. We also present the temperature dependence for junctions with different structures in order to rule out possible artefacts and determine the effects of molecular structure on the electron transfer mechanism.

2. Experimental details

Pyrolysed photoresist films (PPFs) were prepared as described in detail elsewhere [28]. Briefly, 0.5 mm lines of photoresist were patterned onto 1.5 cm × 2 cm Si chips that have an insulating thermal oxide layer using standard photolithographic techniques. A positive resist was used (AZ4330) along with a soft-contact chromium/glass mask. After UV exposure and development, the patterned films were pyrolysed in a tube furnace by ramping the temperature to 1100 °C (10 °C min^{-1}) and holding for 1 h under a constant 1000 sccm flow of 5% H_2 in N_2 (forming gas). After cooling to room temperature with a continual flow of forming gas, the samples were removed and modified by diazonium reduction.

PPF was modified with thin (1–5 nm) molecular layers by using each sample as a working electrode in a 1 mM solution of a diazonium ion precursor with 0.1 M tetrabutylammonium tetrafluoroborate as the supporting electrolyte in acetonitrile. The reduction of the diazonium ion, which leads to radical formation and subsequent covalent surface bonding of the molecule, was controlled by the application of a potential sweep programme, enabling control over the molecular layer thicknesses. For nitroazobenzene (NAB), biphenyl (BP), and nitrobiphenyl (NBP) diazonium reagents, the same potential limits were used (+0.4 to −0.6 V) for a set number of cycles in order to produce films of the desired thickness. For fluorene (FL), the negative limit was extended to −0.8 V, and a single cycle applied. In all cases, the sweep rate was 200 mV s^{-1}. Thicknesses were measured using a previously reported AFM scratching technique [15, 33], where a trench made in contact mode AFM is imaged in tapping mode in order to analyse the depth of the scratch. Using NAB as an example, one voltammetric cycle yields a 2.6(±0.3) nm film and four cycles a 4.5(±0.3) nm film. Other film thicknesses are as indicated throughout the text. Chemical structures and abbreviations for all molecules utilized in this work are shown in figure 1(A).

Top contacts were deposited onto the modified PPF to result in the junction structure depicted in figure 1(B). 30 nm of copper (0.3 nm s^{-1}) followed by 15 nm of Au (0.1 nm s^{-1}) were evaporated through a shadow mask with 0.1 or 0.5 mm wide openings oriented at 90° to the PPF lines. The junction area was defined by the overlapping regions of the modified PPF and the Cu metal. The inset in figure 1(B) shows an idealized model of the PPF–molecule–Cu sandwich at

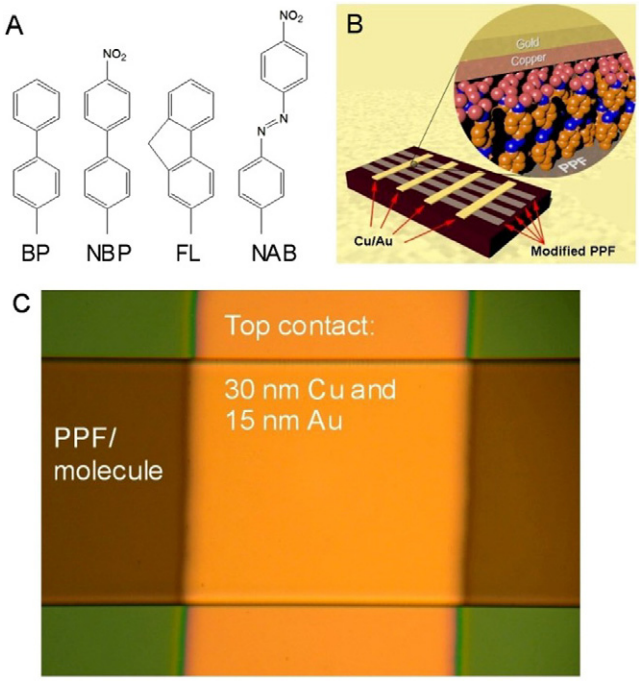

Figure 1. (A) Molecular structures and abbreviations for adlayers used in this study (BP, biphenyl; NBP, nitrobiphenyl; FL, fluorene; NAB, nitroazobenzene). (B) Schematic representation of carbon–molecule–copper junction where each point at which a metal stripe crosses the PPF is a single junction. The inset in (B) shows an idealized molecular level depiction of the layered structure of the cross-junction. (C) Micrograph of an actual junction showing the top contact stripe oriented vertically across the horizontal PPF/molecule strip. The bias voltage is applied by contacting micromanipulator-controlled probes on the PPF and top contact immediately adjacent to the junction.

(This figure is in colour only in the electronic version)

each intersection. Deposition was carried out via electron-beam evaporation. The oxygen or argon partial pressure was controlled by admitting high-purity O_2 or Ar into the chamber to the desired pressure and was monitored using a residual gas analyser (Stanford Research Systems RGA/200).

The electrical properties of the junctions were tested in ambient air within one week of fabrication using custom built probe stations with three or four tungsten probes. In-house instruments were constructed with National Instruments DAQ boards and programmed with Labview software that was designed to execute voltage sweeps and record the resulting current. A three- or four-wire configuration was used that applies a voltage between the PPF (wire 1) and a top contact (wire 2), with a voltage sensing probe (wire 3) placed on the opposite side of the junction in contact with the PPF. This third lead corrects for ohmic losses due to the non-negligible resistance of the PPF bottom electrode. The measured current is recorded from wire 2 with an SRS 570 current amplifier, and plotted versus the voltage read at wire 3. A fourth wire that compensates for losses in the metal top contact was also used in some instances. A Gamry Reference 600 potentiostat was used in three-wire configuration for assessments of lower resistance junctions (i.e. where >6 mA results at ±0.5 V), and it was verified that both instruments yielded identical results for mutually accessible regions. All probes were controlled with three-axis micromanipulators. In all cases, the current density–voltage curves are plotted assuming that the junction area is defined by the geometric measurements of the PPF stripe (0.05 cm) and the dimensions of the shadow mask used in Cu deposition (0.01 or 0.05 cm).

The temperature dependence of junction conductivity was measured using a Janis ST-500 cryogenic probe station. Sample chips were loaded into a turbomolecular-pumped vacuum chamber and the pressure reduced to $<10^{-4}$ Torr before collecting j–V curves using micromanipulator-controlled probe needles connected with pass-through BNC cables. After evacuation, liquid nitrogen was pumped through the sub-stage compartment to cool the sample. A heating element combined with a thermocouple-based temperature controller (Scientific Instruments model 9700) maintained the set-point temperature in the range from 100 to 400 K, with better than 0.5 K accuracy.

3. Results and discussion

3.1. General device behaviour

The idealized representation of a cross-junction shown in figure 1(B), as discussed previously, shows a molecular layer sandwiched between two conductors (PPF and Cu). Each area at which the PPF crosses the Cu can therefore serve as a molecular junction by applying a bias voltage across the ensemble of molecules. The photomicrograph in figure 1(C) shows one such cross-junction, where the PPF and top contact lines are 0.5 mm in width. The notation for describing carbon–molecule–Cu devices follows a layer format going from bottom to top, and the thickness of the molecular coating in nanometres is given in parentheses. Thus, PPF/NAB(4.5)/Cu expresses a junction with a 4.5 nm layer of NAB bonded to PPF, and a Cu top contact where 30 nm of Cu is followed by 15 nm of Au. This design ensures that Cu is in direct contact with the molecule, while the upper Au film ensures good electrical contact to the measurement probe tips.

Figure 2(A) shows current density–voltage (j–V) curves for three junctions: PPF/Cu, PPF/NAB(2.6)/Cu, and PPF/NAB(4.5)/Cu. For the NAB-containing devices, a plot of $\ln j$ versus V is shown in figure 2(B) to facilitate direct comparison. The curves in figure 2 show several important features. First, with the molecule absent, the value of the resistance ($\sim 10 \pm 5\ \Omega$) is independent of voltage and is much lower than that for junctions containing NAB. In contrast, both NAB junctions show nonlinear j–V curves, with low voltage (±0.1 V) differential resistances of 500 and 1015 Ω for the PPF/NAB(2.6)/Cu and PPF/NAB(4.5)/Cu junctions shown in figure 2, respectively (both junctions have a geometric area of 5×10^{-4} cm^2). The differential resistance (±0.1 V) decreases considerably at voltage magnitudes greater than ∼0.5 V, and is 11 Ω for PPF/NAB(2.6)/Cu and 75 Ω for PPF/NAB(4.5)/Cu at +0.8 V. The reproducibility for these junctions is illustrated by the error bars in figure 2(A) (±one standard deviation for at least three junctions on each chip). These results correspond to relative standard deviation (RSD) values for j

Table 1. Junction resistance and pressure for BP junctions, and a comparison of various junctions.

Junction	P_{total} (Torr)	RGA (Torr) O_2	RGA (Torr) Ar	$R(\pm 0.1$ V, k$\Omega)$	$R \times A$ (Ω cm^2)	Ref.
BP(1.5)/Cu	1×10^{-6}	$<10^{-7}$	—	0.16(±0.02)	0.08	—
BP(1.5)/Cu	1×10^{-5}	$<10^{-7}$	—	0.20(±0.02)	0.10	—
BP(1.5)/Cu	5×10^{-5}	$<10^{-7}$	—	4.02(±0.7)	2.0	—
BP(1.6)/Cu	2×10^{-7}	—	—	6.8	3.1	[15]
NAB(4.5)/Cu	2×10^{-6}	$<10^{-7}$	—	1.0(±0.3)	0.5	—
NAB(4.5)/Cu	1×10^{-5}	1×10^{-5}	—	19(±3)	9.5	—
NAB(2.6)/Cu	2×10^{-6}	$<10^{-7}$	—	0.50(±0.1)	0.25	—
NAB(2.6)/Cu	2×10^{-5}	$<10^{-7}$	2×10^{-5}	5.2(±0.7)	2.6	—
NAB(3.7)/Cu	—	—	—	1.5	2.9	[22]
FL(1.4)/Cu	1×10^{-6}	—	—	0.87	2.2	
FL(1.7)/Cu	2×10^{-7}	—	—	0.7	0.32	[15]
NBP(2.0)/Cu	1×10^{-6}	—	—	0.25	0.63	
NBP(3.7)/Cu	1×10^{-6}	—	—	222	555	
NBP(2.1)/Cu	2×10^{-7}	—	—	1.3(±0.08)	0.59	[15]
NBP(3.8)/Cu	2×10^{-7}	—	—	43.4(±1.5)	20	[15]

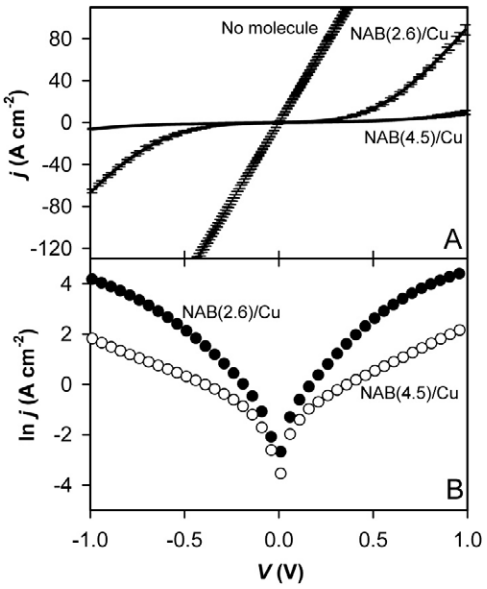

Figure 2. (A) j–V curves for three junctions: PPF/Cu, PPF/NAB(2.6)/Cu, and PPF/NAB(4.5)/Cu. The error bars represent ±one standard deviation for three to five junctions. (B) ln j versus V plot for the molecule-containing junctions. Sweep rate 10^3 V s^{-1}, geometric junction areas 5×10^{-4} cm^2.

of less than 20% for the entire voltage range and under 10% for $V < \sim 0.5$ V. The yield, defined as the percentage of junctions that are distinct from the PPF/Cu junctions and give j–V curves within three standard deviations of the average across an entire chip (four to eight junctions), exceeds 80%. For example, out of 57 PPF/NAB(4.5)/Cu junctions on eight samples, 47 gave j–V curves that fall within one standard deviation of the average. Of the remaining ten devices, four were short circuits, matching the curve obtained for the PPF/Cu junction, while the final six gave an 'anomalous' response that fell outside 3σ, but were less conductive than the PPF/Cu device. We shall return to a discussion of reproducibility and yield later. These findings are in good agreement with previous results [15, 22] and demonstrate a definite electronic signature for the molecule. That is, the presence of a molecular layer induces a significant change in the j–V curve, and the current is a strong function of film thickness. However, there are several details of device fabrication that can also impact electronic behaviour, as discussed in more detail below.

From the data in figure 2, we can consider what gives rise to the j–V characteristics of PPF–molecule–Cu junctions. Clearly, the junctions containing molecules have electrical properties that are distinct from control devices. However, a common concern that arises when considering electron-beam evaporation of top contact metals onto molecular layers is the possibility that pinholes in the adlayer and/or that damage of the molecular layer during deposition lead to an array of metallic filaments, or 'short circuits'. A second concern when using Cu as a top contact metal is the formation of Cu oxides, which would impact the electronic properties of the junctions. Both of these issues will be addressed in the following sections.

3.2. Role of copper oxides

Although a set of junctions prepared during a single deposition show high reproducibility (see the error bars in figure 2), fluctuations of the current magnitude were occasionally observed from batch to batch. That is, current densities for two PPF/NAB(4.5)/Cu junctions prepared at different times could vary by as much as a factor of 20 in either direction for extreme cases. However, we found that in order to replicate the j–V characteristics from batch to batch the atmosphere during Cu deposition must be closely controlled. Higher chamber backpressure correlated consistently with lower current densities in the finished devices. Table 1 lists the low voltage (±0.1 V) resistance, as determined from the inverse slope of the i–V curve, for several junctions as a function of deposition pressure (including junctions for which gases were added intentionally and also a collection of values obtained previously from our group [15, 22]). As an example, for PPF/BP(1.5)/Cu junctions, when the total pressure is less than $\sim 10^{-5}$ Torr, the resistance value is 160–200 Ω, while a

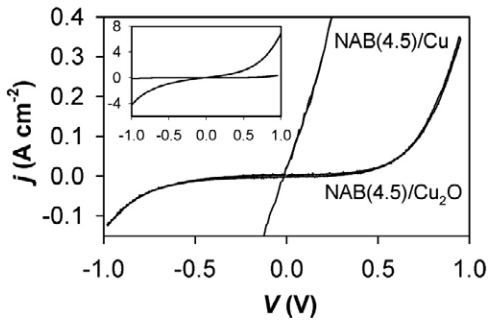

Figure 3. Comparison of PPF/NAB(4.5)/Cu(30) and PPF/NAB(4.5)/Cu_2O(30) junctions. Sweep rate 10^3 V s^{-1}, geometric junction areas 5×10^{-4} cm^2.

pressure of 5×10^{-5} Torr resulted in much higher resistance (4000 Ω). Similar results were obtained for other devices, where backpressure had minor effects on resistance when at or below 10^{-5} Torr, while higher pressures caused increased resistance. The results shown in table 1 also confirm the strong effect of molecular layer thickness on junction conductance, reported previously for similar devices [15].

One obvious factor that could induce such changes is oxidation of Cu metal by trace gases to produce semiconducting Cu oxide. To investigate the effect of pressure on junction conductance, variations on metal deposition conditions were explored, including Cu_2O as a top contact, introducing oxygen and argon during deposition, and XPS was carried out on a variety of samples prepared under different conditions. Figure 3 shows j–V curves for PPF/NAB(4.5) with either Cu(30) or Cu_2O(30) as the top contact. The Cu_2O sample also had 5 nm Cu and 15 nm Au as a conductive upper layer for making contacts while the Cu sample had only the additional 15 nm Au. The 5 nm Cu layer was deposited to minimize Au penetration into the Cu_2O layer. Intentional deposition of Cu(I) oxide yields devices with significantly lower current and a different shape than that obtained for Cu junctions, in agreement with observations for other metal oxide top contacts [16, 22, 23]. The difference in resistivity between metallic and oxidized Cu is significant, covering at least ten orders of magnitude at room temperature [43]. Deposition of metallic Cu never produced junctions with j–V characteristics similar to the copper oxide devices. The significant differences in these curves are a preliminary indication that modulation of junction conductivity is not a direct consequence of oxide formation. This assertion was tested by fabricating junctions in environments with intentionally added gases.

Figure 4(A) shows ln j versus V curves for NAB(4.5)/Cu junctions prepared with high ($>10^{-5}$ Torr) and low ($<10^{-7}$ Torr) levels of oxygen in the evaporation chamber during top contact deposition, as determined with the RGA. The shapes of the curves in figure 4(A) are very similar, but there is a significant difference in the overall current density, with the higher oxygen pressure producing close to a 20-fold decrease in current. Although this result might imply that Cu_2O formation during deposition decreased the junction conductance, a very similar effect is observed with Ar instead of O_2, as shown in figure 4(B) for a set of

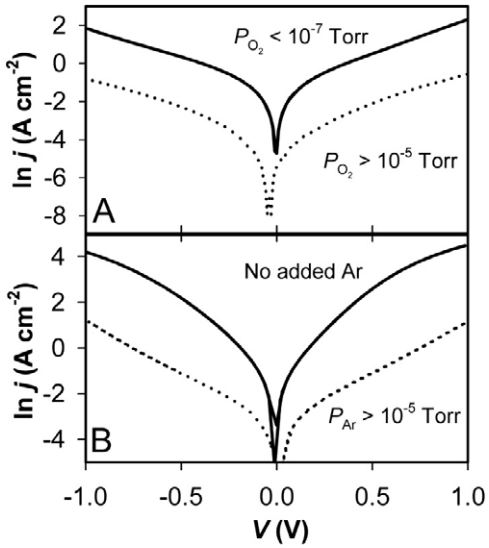

Figure 4. (A) ln j versus V curves for PPF/NAB(4.5)/Cu junctions where the oxygen pressure was $<10^{-7}$ Torr throughout top contact deposition (solid curve) and where P_{O_2} was $\sim 10^{-5}$ Torr (dotted curve). (B) ln j versus V curves for PPF/NAB(2.6)/Cu junctions in the absence of added Ar (solid curve, O_2 pressure was $<10^{-7}$ Torr) and in $\sim 10^5$ Torr Ar (dotted curve, O_2 pressure was $<10^7$ Torr). Sweep rate 10^3 V s^{-1}, geometric junction areas 5×10^{-4} cm^2.

NAB(2.6)/Cu junctions (i.e., Ar caused a $\sim 20\times$ decrease in the current density). These results are also summarized in table 1, where the low voltage (±0.1 V) resistance values are listed, illustrating that total pressure, and not oxygen pressure, modulates the conductance of the device.

XPS was used to characterize the level of oxygen present in Cu samples prepared in the same way as the molecular junctions but without the top 15 nm of Au. Data are in the supplemental material (available at stacks.iop.org/JPhysCM/20/374117), and we summarize here. Four samples were tested: freshly prepared PPF/Cu, PPF/Cu that was exposed to air for 151 days, PPF/Cu prepared with oxygen leaked into the chamber such that the pressure of O_2 was $>10^{-5}$ Torr during deposition, and PPF/Cu_2O. In all cases, Ar ion etching was used to profile oxygen through the 30 nm thickness of the Cu film. The results of these experiments showed that oxide is only detectable in two cases: the Cu_2O sample, and the aged sample. For the aged sample, oxygen was present at a detectable level only in the top $\sim$ 5 nm of Cu (which had been exposed to air), while the copper(I) oxide sample showed oxygen throughout the entire depth. Although Ar^+ etching can remove oxygen preferentially over Cu, causing a decrease in the intensity of the O 1s peak as etching proceeds [44], the results clearly demonstrate that oxygen was only present at a trace level 5 nm or more below the surface for all cases except the sample prepared using a Cu_2O source as a control, which showed an O 1s peak until the etch depth was >30 nm. Our XPS results are also consistent with a recent study on the growth of Cu oxides at thin Cu films upon exposure to ambient conditions [45]. In this study, the native oxide thickness was found to be less than 6.0 nm for films exposed to air for up to 122 days. Taken together with the

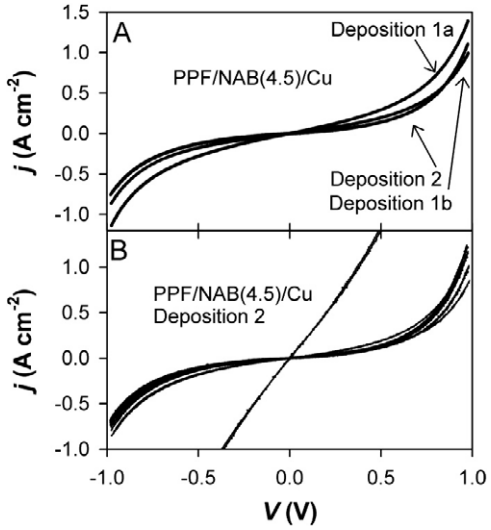

Figure 5. (A) Averages for three different PPF/NAB(4.5)/Cu samples. Deposition 1 was carried out with two different PPF/NAB(4.5) samples in the chamber at the same time (1a and 1b). A second evaporation (deposition 2) was carried out independently, with every attempt to maintain identical conditions (pressure, rate, etc). (B) Overlay of all seven junctions from one chip (deposition 2), illustrating the criteria for rejection of one junction (yield 6/7). Sweep rate 10^3 V s^{-1}, geometric junction areas 2.5×10^{-3} cm^2.

Table 2. Table of data for three PPF/NAB(4.5)/Cu junctions: two from a single deposition (1a and 1b) and a third from a second deposition (2) where the conditions were kept as constant as possible. Junction area = 0.0025 cm^2.

Sample-deposition	Junction	R(±0.1 V, kΩ)	j(0.5 V, A cm^{-2})
PPF/NAB(4.5)/Cu-1a	1	0.95	0.254
	2	1.0	0.256
	3	0.79	0.352
	4	0.89	0.279
	5	0.80	0.320
Average		0.89(±0.09)	0.29(±0.04)
PPF/NAB(4.5)/Cu-1b	1	1.30	0.213
	2	1.35	0.205
	3	1.27	0.215
	4	1.40	0.182
	5	1.60	0.178
Average		1.3(±0.1)	0.20(±0.02)
PPF/NAB(4.5)/Cu-2	1	1.55	0.199
	2	3.78	0.115
	3	4.18	0.125
	4	3.80	0.142
	5	2.81	0.150
	6	0.163	1.4
	7	2.11	0.135
Average		3(±1)	0.14(±0.03)

characterization of junction conductance, the XPS experiments show that copper oxide did not significantly contribute to junction behaviour for the conditions used to make junctions unless it is introduced intentionally through direct deposition of Cu_2O.

Although we do not fully understand the environmental effect on junction conductance, a possible origin is variation of microscopic contact area with deposition backpressure. Modulation of the kinetic energy of the Cu by collisions with chamber gases is unlikely, since the mean free path is at least 90 cm for all pressures employed, or about four times the target to sample distance. However, collisions between chamber gases and the molecular layer surface during formation of the Cu top contact could lead to incomplete contact between the Cu and molecular layers. We are currently designing additional experiments to confirm this tentative conclusion. However, since junction conductivity varies little for pressures below 10^{-5} Torr, we conducted experiments to test if junction conductivity is consistent from batch to batch when the deposition environment is carefully monitored.

Figure 5(A) shows overlays of the averages of five to seven junctions from each of three different samples. The j–V curves labelled deposition 1a and 1b are averages obtained from two identical PPF/NAB(4.5) samples subjected to top contact deposition during a single evaporation where the total pressure was $\sim 5 \times 10^{-6}$ Torr. The j–V curve in figure 5(A) labelled deposition 2 is for a third PPF/NAB(4.5) chip, identical to the first two chips, but where the top contact deposition was carried out during an independent evaporation. For this second deposition, every effort was made to ensure that the conditions were as close as possible to those during the first deposition. These data illustrate that junctions with reproducible behaviour can be obtained both from sample to sample and from batch to batch if the conditions during evaporation are controlled closely. To further illustrate reproducibility and yield, figure 5(B) shows an overlay of all seven junctions from deposition 2. Only a single junction gave an 'anomalous' response, where it can be seen that a much higher current density is observed, even though there is still some curvature (i.e., the anomalous curve does not approach the PPF/Cu response of figure 2(A)). The data in figure 5 are summarized in table 2, where the low voltage (±0.1 V) resistance value and the current density at 0.5 V are listed for each junction for all three cases. Samples 1a and 1b gave 100% yield, while sample 2 gave 86% yield (6/7). Moreover, the resistance values fall within a factor of three of each other, illustrating the batch-to-batch and chip-to-chip reproducibility for PPF–molecule–Cu junctions. The data for the second deposition also illustrate that in one junction anomalous behaviour similar to that expected for metallic short-circuit filaments was observed. A more critical analysis of filament formation is presented below.

3.3. Critical assessment of filaments

After establishing that Cu oxides do not control the electronic properties of PPF–molecule–Cu junctions prepared using a metallic Cu source, we return to the original consideration of what gives rise to the j–V characteristics of PPF–molecule–Cu junctions. A critically important issue in junctions where the metallic conductor is deposited by vapour deposition is the possibility that an array of short-circuit filaments results from penetration of the Cu into the molecular layer, either through pinholes or by damaging the molecular layer. At

a certain level of filament density, the response should approach that for a PPF/Cu junction where no molecular layer is present at all (i.e. a linear j–V curve; figure 2, 'no molecule' case). However, the concern arises when the total cross-sectional filament area is small compared to the junction area, leading to an intermediate effect. Fortunately, there are several easily identified hallmarks of filament-based conduction that can be used to evaluate whether the observed current density–voltage (j–V) curve is dominated by direct PPF–metal contacts.

We define a 'filament' as direct Cu to PPF contact in one or more locations, effectively creating a short circuit which bypasses the molecular layer. The resistivities of the materials used as bottom and top contacts have well defined temperature dependences that can be used to evaluate the possibility of filament-based conduction. Table 3 lists the temperature coefficients of resistivity for Cu, PPF, glassy carbon (GC, which is similar to PPF in many ways [28]), and a PPF/Cu device. First, the resistivity of Cu increases with increasing temperature (j decreases), while PPF and GC show an opposite trend. Second, the temperature dependence of a PPF/Cu/Au sample measured in three-wire mode is close to that of Cu metal. This result is expected, since the three-wire geometry corrects for the resistance of PPF but not for Cu/Au. The temperature dependence of molecular junctions, discussed in more detail below, shows two results that are in contrast to filament-based conduction: three molecules show temperature-independent behaviour at low temperatures (<250 K), and an increase in conductance with temperature above 250 K. This behaviour is opposite that expected for conduction by Cu filaments. Finally, the temperature dependences measured in either three-wire or four-wire modes show the same trends. In four-wire mode, where both the resistance of the PPF and the Cu are corrected (and therefore changes in resistance of the contacts as a function of temperature are also accounted for), the temperature dependence represents that for the molecular layer. In three-wire mode, on the other hand, the same trend is observed, indicating that the resistance of the Cu top contact is negligible compared to the much higher resistance of the molecular layer. Collectively, these results indicate that junction temperature dependence is distinct from that expected for metal filaments, and that filament conduction is an unlikely mechanism for junction conductance.

An additional strong argument against conduction by filaments involves the filament dimensions necessary to explain the observed junction resistance. For example, a junction with a resistance of 1 kΩ (e.g., see table 2) requires a Cu filament with a diameter of 0.3 nm if the 'wire' length is 4.5 nm (the molecular layer thickness) and it has the bulk resistivity of Cu (1.7×10^{-6} Ω cm at room temperature [43]). The current density through this filament would exceed 10^{11} A cm^{-2}, and resistive heating would raise the filament temperature to above the melting point of Cu in well under a nanosecond after the application of a bias of less than 0.1 V. If there were more than one Cu filament present, they would need a smaller diameter to account for the observed resistance, and would be similarly unable to support the resulting current density and heating rate. A quantized conductance model with 12.9 kΩ filaments leads to a similar result in that enormous current densities would result through such structures. We conclude that a model which attempts to explain the observed junction resistance with metal filaments is unrealistic, and results in unsupportable current densities and filament heating rates.

Table 3. Temperature dependence of the resistivity of various materials relevant to the present work.

Material/device	Temperature coefficient (Ω cm K^{-1})[a]
Cu[b]	$+6.8 \times 10^{-9}$
PPF[c]	-1.99×10^{-6}
Glassy carbon[d]	-1.25×10^{-6}
PPF/Cu/Au	$+4 \times 10^{-9}$

[a] Values of ρ versus T obtained from literature or experimentally measured.
[b] Literature value [43].
[c] Determined by measuring the resistance of a PPF stripe 1 μm in height, 5 mm wide, and over a total length of 0.7 cm (probe spacing).
[d] Literature value [49].

3.4. Electron transfer mechanisms

To investigate the effects of molecular structure on junction conductance, six samples of PPF modified with different molecular layers were subjected to simultaneous top contact deposition (pressure 10^{-6} Torr and rate of 0.3 nm s^{-1}), in order to reduce variations in junction behaviour caused by deposition parameters. Figure 6 shows an overlay of six j–V curves (ln j versus V is shown in the inset) for a batch of junctions having identical top and bottom contacts, but a variety of different molecular layers (or no molecule). For these samples, the top contact was deposited simultaneously onto all samples. Error bars represent ±one standard deviation for at least three junctions on each chip, and the thicknesses indicated in the legend are accurate to ±0.3 nm. It is apparent from figure 6 that different molecules show distinct j–V curves. For example, comparing molecular layers with similar thicknesses, it is apparent that NBP is the most conductive, while BP and FL are slightly less conductive than NBP, but similar to each other (within the experimental error). On the other hand, when the thickness of the molecular layer was varied, in all cases the thicker layer produces higher resistance.

Given the uncertainty about real contact area revealed by the pressure dependence discussed earlier, it is useful to consider analysis methods which are independent of area. For a nanoscopic film sandwiched between two conductors, several electron transfer mechanisms are possible [21]. For example, if the thickness of the film is sufficiently thin, electrons can tunnel from one conductor to the other. However, when the voltage bias between the two conductors becomes large enough to approach the tunnelling barrier height, a transition to field emission can take place [46]. In order to confirm this mechanistic picture, experiments as a function of temperature can be carried out; current due to tunnelling or field emission is independent of temperature [21]. Thus, the j–V curves for different molecules and thicknesses were analysed according to a theoretical expression for the tunnelling to field emission

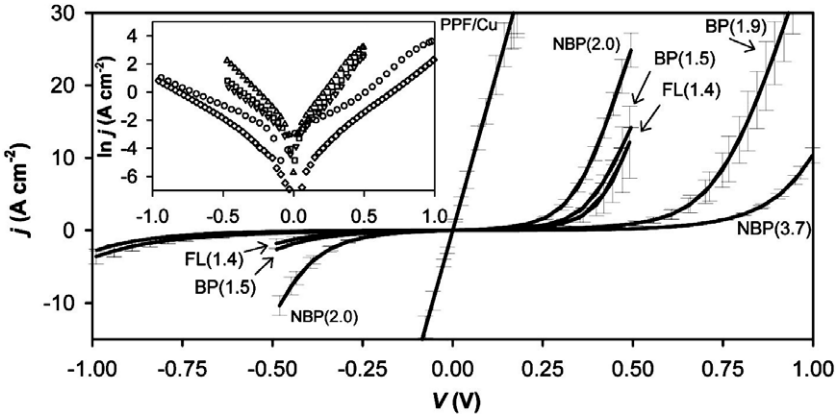

Figure 6. j–V curves for several different junctions, where the top contact was deposited onto all samples in a single process. The labels give the identity and thickness of the molecular layer for each curve. In the inset, the ln j versus V curves are shown where △ is NBP(2.0), □ is FL(1.4), ▽ is BP(1.5), ○ is BP(1.9), and ◇ is NBP(3.7). Sweep rate 10^3 V s^{-1}, geometric junction areas 2.5×10^{-3} cm^2.

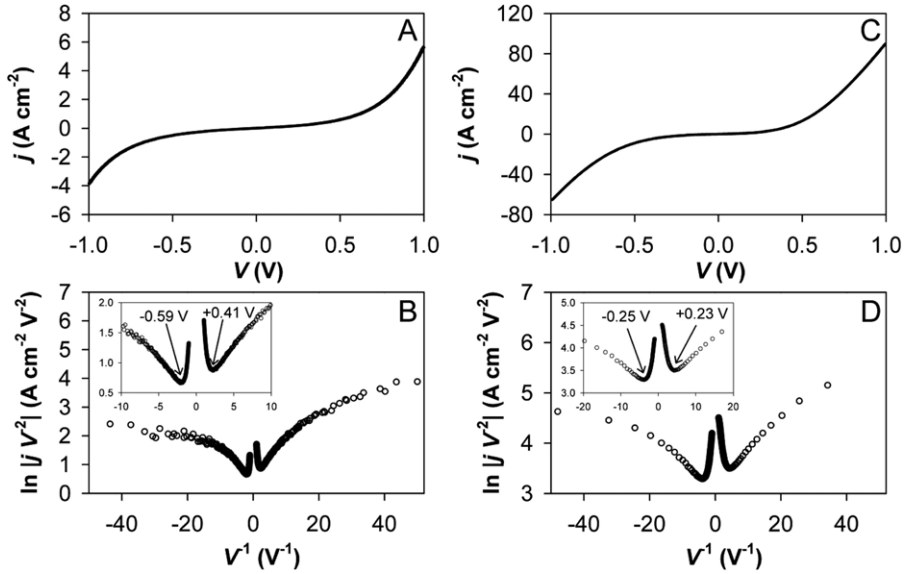

Figure 7. (A) j–V curve for a PPF/NAB(4.5)/Cu junction. (B) Plot of $\ln|jV^{-2}|$ versus V^{-1} for the data in (A). (C) and (D) are corresponding plots for PPF/NAB(2.6)/Cu. The minima in $\ln|jV^{-2}|$ correspond to the transition from tunnelling to field emission, and therefore are a rough measure of the molecular barrier height. For NAB(4.5)/Cu, V_{trans} values (the peak locations) are +0.41 V and −0.59, which correspond to transition electric field values of +0.9 and −1.3 MV cm^{-1}, respectively. For NAB(2.6), the analysis gives +0.23 and −0.25 V, or +0.88 and −0.96 MV cm^{-1}, respectively. Sweep rate 10^3 V s^{-1}, geometric junction areas 5×10^{-4} cm^2.

transition [46], and in a few cases the temperature was varied in the range from 100 and 450 K.

Figure 7(A) shows a j–V curve for one PPF/NAB(4.5)/Cu junction that is representative of many made under similar conditions. Figure 7(B) shows a plot of $\ln|jV^{-2}|$ versus V^{-1} for the data shown in figure 7(A). To illustrate the response obtained for a different thickness, figure 7(C) shows a j–V curve for a single NAB(2.6)/Cu junction, and figure 7(D) the corresponding $\ln|jV^{-2}|$ versus V^{-1} plot. The peak-like features in figures 7(B) and (D) are attributed to the bias at which the voltage is sufficient to induce field emission [46], which is different in figures 7(B) and (D) due to the different layer thicknesses. For junctions of various molecules and thicknesses, the field emission analysis yielded plots with shapes similar to that shown in figures 7(B) and (D) with the exception of a very thin layer (1.7 nm) of NBP, which showed no transition. We attribute this observation to the fact that NBP shows the lowest of the measured barrier heights (see below), and therefore a very thin layer of NBP either allows field emission at very low voltages (i.e., the transition value is not accessible from this curve), or linear tunnelling is efficient enough to mask the transition. In any case, thicker layers of NBP showed a clear transition, similar to that observed in figure 7.

A simplistic interpretation of the transition voltage is that the electric field strength is sufficient to overcome the tunnelling barrier, and therefore electrons can be easily transmitted across the molecular layer. At this point, the current begins to increase rapidly, as in figures 7(A) and (C). Importantly, the plot of $\ln|jV^{-2}|$ versus V^{-1} in figures 7(B)

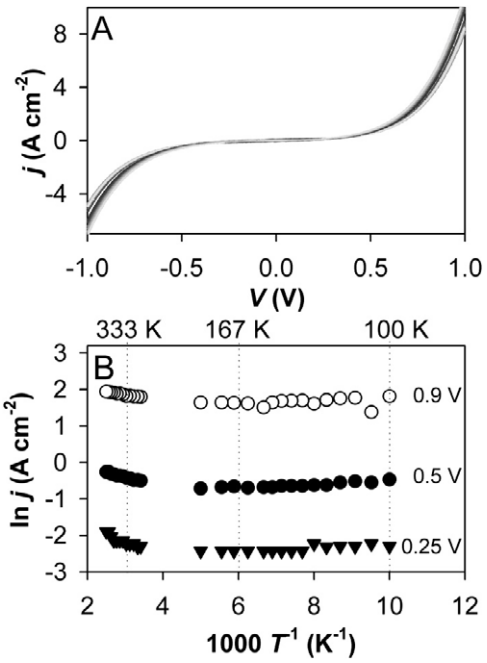

Figure 8. (A) j–V curves for PPF/NAB(4.5)/Cu as a function of temperature in the range 100–400 K. Negligible temperature dependence is observed at low temperature (<200 K), with a slight increase in j at higher temperatures. (B) Arrhenius plot for the data in (A) at three different voltages. Linear regression analysis for the higher temperature range yielded barrier values of 0.02–0.04 eV. Sweep rate 10^3 V s^{-1}, geometric junction area 5×10^{-4} cm^2.

Table 4. V_{trans} and E_f–E_{HOMO} data.

Junction	V_{trans} (V)	E_{trans} (MV cm^{-1})	E_f–E_{HOMO} (eV)[a]
NBP(1.7 ± 0.3)	—	—	—
NBP(2.8 ± 0.3)	0.26(±0.05)	0.92	—
NBP(3.8 ± 0.2)	0.45(±0.1)	1.18	—
BP(1.9 ± 0.3)	0.35(±0.05)	1.84	1.5
FL(1.8 ± 0.3)	0.27(±0.04)	1.5	1.4
NAB(2.6 ± 0.3)	0.27(±0.03)	1.0	1.1
NAB(4.5 ± 0.4)	0.45(±0.08)	1.0	1.1

[a] Determined from ultraviolet photoelectron spectroscopy (see supplemental supporting information available at stacks.iop.org/JPhysCM/20/374117).

and (D) enables a clearer estimation of the barrier height than a j–V curve due to the peak-like feature. Note also that in figures 7(B) and (D) the values of the transition voltages are distinct for different polarity: its magnitude is always higher when PPF is biased negative. This observation held for all junctions for which this analysis was carried out.

Table 4 lists transition voltages and electric fields for four different molecules and various thicknesses of NAB and NBP. E_{trans} is much less dependent on molecular layer thickness than V_{trans}, consistent with a field-rather than bias-driven mechanism. Ultraviolet photoelectron spectroscopy (UPS) measurements of the energy gap between the Fermi level and the molecular HOMO (E_f–E_{HOMO}) were determined from the onset of the UPS peak for four samples (see supplemental supporting information available

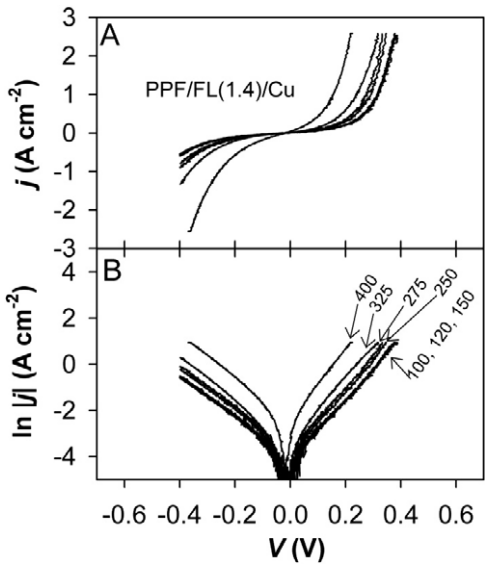

Figure 9. (A) j–V curves for PPF/FL(1.4)/Cu as a function of temperature in the range 100–400 K. Sweep rate 10^3 V s^{-1}, geometric junction area 2.5×10^{-3} cm^2.

at stacks.iop.org/JPhysCM/20/374117). The trend for the transition electric field values and the E_f–E_{HOMO} data tends in the same direction (both go from smallest to largest in the order NAB, FL, then BP), serving as an indication that the values of E_{trans} correlates with molecular orbital energies. So far, the analysis of j–V curves is supportive of a tunnelling-to-field emission mechanism. However, we have had difficulty fitting experimental j–V data directly to theoretical expressions for this charge transfer mechanism. Thus, in order to provide additional insight into possible electron transfer modes, the temperature dependence of j–V curves was measured for several devices.

Figure 8(A) shows plots of j–V curves for PPF/NAB(4.5)/Cu obtained at temperatures of 100–400 K. Figure 8(B) shows the corresponding Arrhenius plot for three bias values. The voltage at which j is observed does not significantly alter the Arrhenius plots, which all show a temperature-independent region from 100 to ∼300 K with an activated region at elevated temperatures. In the high temperature (>250 K) region of the plot, a calculation of the empirical barrier yields 0.03±0.01 eV for NAB(4.5). These data are qualitatively similar to our previous measurements on ensemble devices [14, 15] and also to a report on conjugated single molecule junctions with gold as both contacts [47]. Experiments similar to that shown in figure 8 were carried out for BP(1.9), NBP(3.7), and FL(1.4), as discussed further below.

Figure 9 shows j–V curves for a PPF/FL(1.4)/Cu junction as a function of temperature. For this molecule, there is still a region of temperature-independent conduction. However, beginning at ∼250 K, there is a more strongly activated region than that observed for NAB. Figure 10 shows Arrhenius plots for four molecular layers over a total temperature range of 100–450 K. In all cases, the changes in current density that are observed were reversible upon temperature cycling, and the j–V curves returned to their original state after

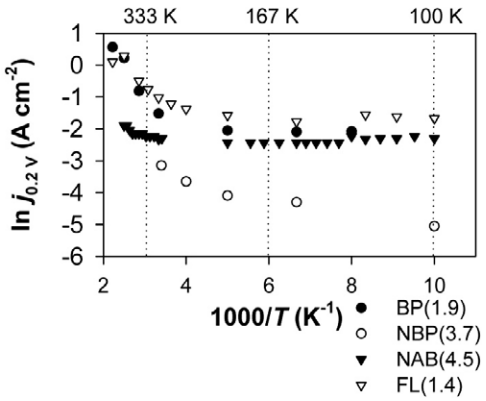

Figure 10. Arrhenius plot for four PPF–molecule–Cu junctions, as indicated in the legend.

the entire temperature excursion. Notably, two samples showed much larger barriers in the higher temperature range compared to the others. BP and FL give barriers of 0.17 and 0.1 eV, respectively, in the linear portion of their Arrhenius plots, while NAB gave a barrier of 0.03 eV. Finally, the NBP junction yielded a barrier of ∼0.02 eV over the entire temperature range. Taken together, the trends of current with temperature support the tunnelling/field emission mechanism below ∼300 K, since tunnelling should be temperature independent. Moreover, the trends of junction conductance with temperature are contrary to what would be observed for metallic filament-based conduction, as discussed above. As noted by many authors, coherent tunnelling should be extremely inefficient across distances greater than ∼2 nm. The temperature independence of conductance for 4.5 nm NAB junctions reported here is therefore surprising if coherent tunnelling is the only operative transport mechanism. However, there are fundamental structural differences between the devices described in this work and the more commonly investigated SAM or Langmuir–Blodgett structures. First, the bonding and electronic coupling between the PPF and the molecule are both strong, with ∼100 kcal mol^{-1} C–C bonds compared to the <40 kcal mol^{-1} Au/SAM and Langmuir–Blodgett bonds. As reported previously, the electronic coupling between NAB and PPF is sufficiently strong to cause a significant red-shift in the UV–vis absorption of chemisorbed NAB relative to that in solution [48]. Second, the Cu top contact has been shown by XPS to form a Cu–N bond upon deposition onto nitro-containing molecules [21], indicating that for NAB and NBP devices both the top and bottom contacts are covalently bonded to the molecular layer. Third, thick films of NBP and NAB can be formed electrochemically on PPF, implying that electron conduction is possible during reduction of the diazonium precursors of these molecules. Stated more generally, the extended conjugation of the multilayer structure may result in the formation of polarons, leading to band transport similar to that in thicker films of conducting polymers. Overall, the combination of strong electronic coupling between molecules and contacts through covalent bonds and the extended conjugation within the molecular layer implies a quite different conduction mechanism from coherent tunnelling, based more on molecular orbitals and band transport than on Simmons tunnelling or superexchange.

4. Conclusions

This paper has addressed electron transfer mechanisms in molecular electronic devices composed of aromatic molecules covalently bound to conductive carbon surfaces with copper metal top contacts. A strong effect of the atmosphere during top contact deposition was found, but the possibility of Cu oxide formation was ruled out as an underlying cause. Instead, we postulate that a change in the microscopic contact area results from collisions of gases with the surface during deposition. In any case, by preparing junctions under closely monitored conditions, the sample-to-sample variation in conductance is a factor of ∼3, which is small enough to enable the observation of structural effects (i.e. the identity and thickness of the molecular layer) on conductance. Furthermore, when the top contact is deposited onto many junctions simultaneously, definite changes in junction conductance with variation of molecular structure are observed. An analysis of the temperature dependence of the junctions is able to rule out filament-based conduction. Moreover, based on the minimal temperature dependence below 250 K, we propose that either field emission or band transport mechanisms contribute to electron transport in these devices. The conjugated structure of the molecular layer and the bonding at the contacts are likely to be important issues which determine the electronic behaviour and transport mechanisms in these devices. Most importantly, the electronic characteristics of these molecular junctions are determined by both the contacts and the molecular layers, including the nature of the bonding and electronic coupling at the interfaces between contacts and molecules. In the case of the large area devices studied here, these properties represent the behaviour of ensembles of large numbers of molecules and a variety of bonding geometries and electronic interactions with the PPF and copper contacts.

Acknowledgments

The expert assistance of Amr M Mahmoud in wire bonding of several samples and insightful discussions regarding electron transfer models with professor S Jiménez Sandoval are gratefully acknowledged. The National Institute for Nanotechnology is operated as a partnership between the National Research Council and the University of Alberta, and is jointly funded by the Government of Canada, the Government of Alberta and the University of Alberta. This work was supported by NSERC. We are grateful to the Alberta Centre for Surface Engineering and Science for acquiring XPS results, and Hong Tian and The Ohio State University Chemistry Department XPS facility for obtaining UPS spectra.

References

[1] McCreery R L 2006 *Anal. Chem.* **78** 3490
[2] Grill L and Moresco F 2006 *J. Phys.: Condens. Matter* **18** S1887

[3] Hipps K W 2001 *Science* **294** 536
[4] Kushmerick J G 2005 *Mater. Today* **8** (7) 26
[5] Zhirnov V V and Cavin R K 2006 *Nat. Mater.* **5** 11
[6] Donhauser Z J, Mantooth B A, Kelly K F, Bumm L A, Monnell J D, Stapleton J J, Price D W, Rawlett A M, Allara D L, Tour J M and Weiss P S 2001 *Science* **292** 2303
[7] Chen J, Reed M A, Rawlett A M and Tour J M 1999 *Science* **286** 1550
[8] Xue Y, Datta S, Hong S, Reifenberger R, Henderson J I and Kubiak C P 1999 *Phys. Rev.* B **59** R7852
[9] Kolipaka S, Aithal R K and Kuila D 2006 *Appl. Phys. Lett.* **88** 233104
[10] Martin C R and Baker L A 2005 *Science* **309** 67
[11] Shimizu K T, Fabbri J D, Jelincic J J and Melosh N A 2006 *Adv. Mater.* **18** 1499
[12] Strachan D R, Smith D E, Johnston D E, Park T-H, Therien M J, Bonnell D A and Johnson A T 2005 *Appl. Phys. Lett.* **86** 043109
[13] Edwards G A, Bergren A J and Porter M D 2007 Chemically modified electrodes *Handbook of Electrochemistry* ed C G Zoski (Boston, MA: Elsevier)
[14] Anariba F and McCreery R L 2002 *J. Phys. Chem.* B **106** 10355
[15] Anariba F, Steach J K and McCreery R L 2005 *J. Phys. Chem.* B **109** 11163
[16] Kalakodimi R P, Nowak A M and McCreery R L 2005 *Chem. Mater.* **17** 4939
[17] McCreery R, Dieringer J, Solak A O, Snyder B, Nowak A M, McGovern W R and DuVall S 2003 *J. Am. Chem. Soc.* **125** 10748
[18] McCreery R L 2004 *Chem. Mater.* **16** 4477
[19] McCreery R L 2004 *Electrochem. Soc. Interface* **13** 46
[20] McCreery R L, Viswanathan U, Kalakodimi R P and Nowak A M 2006 *Faraday Discuss.* **131** 33
[21] McCreery R L, Wu J and Kalakodimi R P 2006 *Phys. Chem. Chem. Phys.* **8** 2572
[22] McGovern W R, Anariba F and McCreery R L 2005 *J. Electrochem. Soc.* **152** E176
[23] Nowak A M and McCreery R L 2004 *Anal. Chem.* **76** 1089
[24] Ranganathan S, Steidel I, Anariba F and McCreery R L 2001 *Nano Lett.* **1** 491
[25] Solak A O, Ranganathan S, Ito T and McCreery R L 2002 *Electrochem. Solid State Lett.* **5** E43
[26] Ssenyange S, Yan H and McCreery R L 2006 *Langmuir* **22** 10689
[27] Wu J, Mobley K and McCreery R L 2007 *J. Chem. Phys.* **126** 024704
[28] Ranganathan S, McCreery R L, Majji S M and Madou M 2000 *J. Electrochem. Soc.* **147** 277
[29] Allongue P, Delamar M, Desbat B, Fageaume O, Hitmi R, Pinson J and Savéant J-M 1997 *J. Am. Chem. Soc.* **119** 201
[30] Bernard M-C, Chausse A, Cabet-Deliry E, Chehimi M M, Pinson J, Podvorica F and Vautrin-Ul C 2003 *Chem. Mater.* **15** 3450
[31] Delamar M, Hitmi R, Pinson J and Savéant J M 1992 *J. Am. Chem. Soc.* **114** 5883
[32] Pinson J and Podvorica F 2005 *Chem. Soc. Rev.* **34** 429
[33] Anariba F, DuVall S H and McCreery R L 2003 *Anal. Chem.* **75** 3837
[34] Kariuki J K and McDermott M T 2001 *Langmuir* **17** 5947
[35] Haick H, Ambrico M, Ghabboun J, Ligonzo T and Cahen D 2004 *Phys. Chem. Chem. Phys.* **6** 4538
[36] Haick H, Niitsoo O, Ghabboun J and Cahen D 2007 *J. Phys. Chem.* C **111** 2318
[37] Akkerman H B, Blom P W M, de Leeuw D M and de Boer B 2006 *Nature* **441** 69
[38] Akkerman H B, Kronemeijer A J, van Hal P A, de Leeuw D M, Blom P W M and de Boer B 2008 *Small* **4** 100
[39] Tran E, Duati M, Ferri V, Mullen K, Zharnikov M, Whitesides G M and Rampi M A 2006 *Adv. Mater.* **18** 1323
[40] Metzger R M 2006 *Chem. Phys.* **326** 176
[41] Selzer Y and Allara D L 2006 *Annu. Rev. Phys. Chem.* **57** 593
[42] Akkerman H B and de Boer B 2008 *J. Phys.: Condens. Matter* **20** 013001
[43] Lide D R (ed) 1996 *CRC Handbook of Chemistry and Physics* 76th edn (New York: CRC Press)
[44] Mencer D E, Hossain M A, Schennach R, Grady T, McWhinney H, Gomes J A G, Kesmez M, Parga J R, Barr T L and Cocke D L 2004 *Vacuum* **77** 27
[45] Platzman I, Brener R, Haick H and Tannenbaum R 2008 *J. Phys. Chem.* C **112** 1101
[46] Beebe J M, Kim B, Gadzuk J W, Frisbie C D and Kushmerick J G 2006 *Phys. Rev. Lett.* **97** 026801
[47] Selzer Y, Cabassi M A, Mayer T S and Allara D L 2004 *J. Am. Chem. Soc.* **126** 4052
[48] Tian H, Bergren A J and McCreery R L 2007 *Appl. Spectrosc.* **61** 1246
[49] Strojnik M 2006 *Unconventional Imaging II*; *SPIE* **6307** S1